Vortex state oscillations in soft magnetic cylindrical dots

K. Yu. Guslienko,[1, *] W. Scholz,[2] R. W. Chantrell,[2] and V. Novosad[1]

[1]*Materials Science Division, Argonne National Laboratory, 9700 S. Cass Ave., Argonne, IL 60439*

[2]*Seagate Research, 1251 Waterfront Place, Pittsburgh, PA 15222*

(Dated: February 2, 2008)

We have studied magnetic vortex oscillations in soft sub-micron cylindrical dots with variable thickness and diameter by an analytical approach and micromagnetic simulations. We have considered two kinds of modes of the vortex magnetization oscillations: 1) low-frequency translation mode, corresponding to the movement of the vortex as a whole near its equilibrium position; 2) high-frequency vortex modes, which correspond to radially symmetric oscillations of the vortex magnetization, mainly outside the vortex core. The vortex translational eigenmode was calculated numerically in frequency and time domains for different dot aspect ratios. To describe the discrete set of vortex high-frequency modes we applied the linearized equation of motion of dynamic magnetization over the vortex ground state. We considered only radially symmetric magnetization oscillations modes. The eigenfrequencies of both kinds of excitation modes are determined by magnetostatic interactions. They are proportional to the thickness/diameter ratio and lie in the GHz range for typical dot sizes.

PACS numbers: 75.40.Gb,75.30.Ds,75.50.Bb,75.75.+a

I. INTRODUCTION

The magnetization vector of a ferromagnetic body (particle) oscillates when variable external magnetic fields are applied. The amplitude of magnetization oscillations, which depends on the intrinsic fields as well as on the particle's geometrical parameters increases drastically when the frequency of the external field coincides with the frequency of a fundamental spin-excitation eigenmode of the system.

This issue has important implications for developing high-speed and high-density magnetic devices, where short field pulses are applied to magnetic media to achieve the magnetization reversal.[1] The characteristic switching time is usually in the nanosecond and sub-nanosecond range for non-uniform and coherent magnetization rotation, respectively. Understanding of spin-wave excitation spectra is thereby crucial to determine the field-dependent spin-instability regions, where spontaneous or thermally-assisted magnetization reversal processes might occur[2].

In the general case, both the short-range exchange and the long-range magnetostatic interactions contribute to eigenfrequencies of the collective spin excitations. The long-wavelength excitations are mainly influenced by dipole-dipole interactions. Therefore, the demagnetizing fields of the magnetic elements determine their eigenfrequencies. These fields can be strongly non-uniform in the case of non-ellipsoidal samples or if the static magnetization distribution differs significantly from the single-domain (collinear) state. This is especially the case for technologically important flat magnetic particles, prepared by means of micro-fabrication and thin film deposition techniques. The adequate description of high-frequency magnetization dynamics in such systems is a challenge for modern magnetism theory.

The remanent magnetization distribution within a ferromagnetic particle is a complex phenomenon that depends on the size and shape of the particle as well as on the balance of different contributions (exchange, magnetostatic, anisotropy etc.) to the magnetic energy. Exchange energy dominates at small particle sizes and favors a uniform magnetization distribution, so-called single-domain or "flower" ("leaf") state. On the other hand, this almost collinear spin alignment leads to large demagnetizing fields due to magnetic surface charges and correspondingly increase of the magnetostatic energy. The importance of the magnetostatic energy increases gradually as the particle size increases. The competition between these two energies and anisotropy energy leads to non-uniform magnetic states such as multi-domain states (if the anisotropy constant is greater than the magnetostatic energy) or magnetic vortices (if the anisotropy energy is small in comparison with the magnetostatic energy). The critical size at which a particle becomes single domain depends on the interplay between the energies mentioned above, and also on the shape of the particle. This critical size is of the order of the material exchange length $L_{ex} = \sqrt{2A/M_s^2}$, where A is the exchange stiffness constant and M_s is the saturation magnetization. A magnetically soft particle with lateral dimensions smaller than the exchange length ($L_{ex} \approx 10 - 20$ nm) is expected to remain in a single domain state at remanence.

Sub-micron magnetic elements with regular shapes (rectangular, cylindrical, spherical etc.) have attracted much attention during the last few years due to considerable progress in fabrication and characterization of the samples.[3,4]

In this paper we will consider dynamic properties of circular particles (dots) made of soft magnetic material with a thickness of about L_{ex} and diameters considerably larger than L_{ex}. It is well established, that a magnetic vortex structure is the ground state of such submicron dots.[5,6,7,8,9,10,11] This vortex state can be interpreted as a

part of a two-dimensional magnetic topological soliton[12] adapted to the particle shape to minimize the total magnetic energy. Experimental studies of the vortex state in flat submicron dots have been performed using different methods. Magnetization reversal in sub-micron dots due to magnetic vortex formation and its displacement has been explored by analytical and numerical micromagnetic modeling.[13,14] It was found from static measurements and calculations that the magnetic vortex state corresponds to a deep energy minimum for submicron dot radii and it can be destabilized either by reducing the dot radius down to the material's exchange length or by applying an in-plane magnetic field. The vortex state is not specific for the circular shape, it was also observed in rectangular,[15] elliptical,[16,17] and triangular[18] flat magnetic elements.

The dynamic properties of sub-micron dots have only more recently attracted some attention.[10] There have been a few successful experimental investigations of the magnetization dynamics under short field pulses in a saturated FeNi disk[19] and also closure-domains in a Co disk.[20] In this article we concentrate on the linear spin dynamics in an equilibrium, but essentially non-uniform, vortex state. Spin excitations in the vortex-state are expected to be substantially different from those in the uniformly magnetized state and also from the excitations (spin-waves) observed in infinite thin magnetic films. An example is the appearance of a low-frequency mode (translation mode) associated with the movement of the vortex as a whole in a potential well created mainly by magnetostatic energy.[21,22] It was found that the vortex core undergoes a spiral motion with the eigenfrequency in the sub-GHz range for thin sub-micron dots. This lowest frequency translation mode can be treated as vortex core excitation and is localized near the dot center. This mode is similar to crossed-domain wall resonance in a magnetic film.[23] We consider that the spectrum of vortex spin excitations will be quantized due to particle's (dot's) restricted geometry as was shown in[24,25] for the saturated state. Spin excitations of the vortex state have been discussed for an infinite film (Ref. 26 and Refs. therein) neglecting the magnetostatic interaction. This is an unsuitable approximation to describe magnetization dynamics of sub-micron magnetic particles, where the exchange contribution to the low-lying eigenfrequencies is essentially smaller than the magnetostatic contribution ($L_{ex} \ll R$, where R is the disk radius). Magnetization dynamics in this case is governed by the long-range dipolar forces. We are not aware of any theoretical or experimental investigation of dipole dominated high frequency spin excitations in a magnetic vortex state except recent results by Novosad et al.[10] and Ivanov et al.[22]

In this paper we address the precessional spin dynamics of the vortex ground state and determine the low-lying vortex eigenfrequencies which correspond to radially symmetric spin excitations. The eigenfrequencies are well above the vortex translation eigenfrequency. Analytical calculations of the eigenfrequencies are supported by numerical micromagnetic simulations.

The vortex magnetization dynamics can be detected, for instance, by ferromagnetic resonance (FMR), Brillouin light scattering (BLS) techniques or by time-resolved Kerr microscopy. The spectrum of the dot discrete eigenfrequencies can be used as a starting point for the consideration of magnetization reversal.

We present in Sec. II a theoretical description and in Sec. III micromagnetic calculations of discrete eigenfrequencies of excitation modes of the vortex state in soft magnetic cylindrical dots. We consider that above the vortex translation mode frequency (which is < 1 GHz) there is a set of radially and azimuthal symmetric modes (of about 10 GHz) localized outside the vortex core. For sub-micron dot sizes the dynamic demagnetizing fields determine the eigenfrequencies of these modes, whereas the translation mode frequency is determined by the static demagnetizing field (magnetostatic contribution to the restoring force). The vortex excitation eigenfrequencies are found from eigenvalues of a magnetostatic integral operator (Sec. II) and also from dynamical micromagnetic simulations (Sec. III) based on the Landau-Lifshitz equation of motion. Full details of the analytical model are reported. Experimental techniques to study these vortex modes are discussed. A comparison of numerical (FEM-BEM and finite differences) micromagnetic simulations with analytical results is presented. Finally, the summary is given in Sec. IV.

II. THEORY

We present a theoretical description of the vortex state oscillations in submicron-size cylindrical dots. Our approach is based on the consideration of small dynamic oscillations over the centered vortex ground state. We consider here only radially symmetric vortex excitation modes in zero applied magnetic field. These modes have frequencies well above the vortex core translation frequency for the given dot sizes. They have maximum FMR and BLS intensity due to their non-zero average dynamic magnetization. It is known that the vortex core bears some topological charges (gyrovector and vorticity, see Ref. 12) and this peculiarity has important consequences for the vortex state dynamics. In the following, we do not consider the vortex charges and assume that the high-frequency excitation modes are localized outside the vortex core. In other words, we neglect the vortex core influence on these modes. Let L denote the dot thickness, and R the dot radius. Since the dot thickness is small, we assume a two-dimensional magnetization distribution $\mathbf{m} = \mathbf{M}/M_s$, $\mathbf{m}^2 = 1$ within the cylindrical dot, which does not depend on the z-coordinate along the dot thickness. We use the angular parameterization for the dot magnetization components $m_z = \cos\Theta$, $m_x + im_y = \exp(i\Phi)\sin\Theta$, $\Phi = \phi \pm \pi/2$. Here positive and negative signs correspond to counter-clockwise and clockwise rotation of the vector $\mathbf{m}$ in the dot plane,

respectively. The cylindrical coordinates ρ, ϕ, z are used below. The spin structure of the static vortex located in the dot center may be described by the one-parameter ansatz

$$\tan(\Theta_0(\rho)/2) = \rho/b \qquad (1)$$

if $\rho < b$ and $\Theta_0 = \pi/2$ if $\rho > b$ as suggested by Usov et al.[27] The radius of the vortex "core" $b \approx 10$ nm can be determined from magnetic energy minimization. The total dot magnetic energy including exchange and magnetostatic energies is:

$$W = L \int d^2\rho [A(\nabla\Theta)^2 + \sin^2\Theta(\nabla\Phi)^2) - \frac{1}{2}\mathbf{H}_m \cdot \mathbf{M}], \qquad (2)$$

where $\mathbf{H}_m$ is the magnetostatic field. We use the equation of motion of variable magnetization

$$-\frac{1}{\gamma}\frac{d\mathbf{m}}{dt} = \mathbf{m} \times (-\frac{\delta W}{\delta \mathbf{m}}) \quad . \qquad (3)$$

The calculation of the exchange contribution to the effective field is straightforward, while the magnetostatic field is expressed via the magnetostatic Green's function[24] in cylindrical coordinates ρ, ϕ, z. The magnetization distribution $\mathbf{m}(\mathbf{r})$ within the cylindrical dot leads to the variable demagnetizing field $\mathbf{h}(\mathbf{r}) = \widehat{G}[\mathbf{m}(\mathbf{r})]$, where $\widehat{G}$ is a tensorial non-local integral operator (the tensorial magnetostatic Green's function $G_{\alpha\beta}(\mathbf{r}, \mathbf{r}')$) expressed in the cylindrical coordinates

$$\widehat{G}[\mathbf{m}(\mathbf{r})] = \int \widehat{G}[\mathbf{r}, \mathbf{r}']\mathbf{m}(\mathbf{r}')d^3\mathbf{r}',$$
$$G_{\alpha\beta}(\mathbf{r}, \mathbf{r}') = -(\nabla_{\mathbf{r}})_\alpha(\nabla_{\mathbf{r}'})_\beta \frac{1}{|\mathbf{r} - \mathbf{r}'|} \qquad (4)$$

We use averaging over z, z' and also over ϕ' (due to the assumed radial symmetry of $\mathbf{m}(\mathbf{r})$). Only $\rho\rho$ and zz-components of the averaged $\widehat{G}$ tensor are not equal to zero. The equation of motion (3) is then linearized by substituting $\mathbf{m}(\rho, t) = \mathbf{m}_0(\rho) + \mu(\rho, t)$ or by magnetization angles:

$$\Theta(\rho, t) = \Theta_0(\rho) + \vartheta(\rho, t), \Phi(\rho, \varphi, t) = \varphi + \frac{\pi}{2} + \psi(\rho, t), \quad (5)$$

where the vector $\mu = (\mu_\rho, \mu_\varphi, \mu_z) = (-\psi \sin\Theta_0, \vartheta \cos\Theta_0, -\vartheta \sin\Theta_0)$ is the dynamic part of the magnetization. For small variables ϑ and $\mu = \mu_\rho = -\psi \sin\Theta_0$ we get a system of two coupled integro-differential equations. We can neglect the dynamic exchange interaction for sub-micron dot radii, exclude the variable $\vartheta(\rho, t)$ and reduce the problem to an eigenvalue problem for the integral magnetostatic operator:

$$\left(\frac{\omega}{\gamma M_s}\right)^2 \mu(\rho) = \int d\rho' \rho' \Gamma(\rho, \rho')\mu(\rho'), \qquad (6)$$

$$\Gamma(\rho, \rho') = \int dr\, r \sin\Theta_0(r) g_{zz}(\rho, r) g_{\rho\rho}(r, \rho'), \qquad (7)$$

where the averaged over thickness Green's function components do not depend on ϕ:

$$g_{\alpha\beta}(\rho, \rho') = \frac{1}{L} \int_0^L dz \int_0^L dz' \int_0^{2\pi} d\phi' G_{\alpha\beta}(\mathbf{r}, \mathbf{r}') \qquad (8)$$

Solution of Eq. (6) yields the eigenfunctions $\mu_n(\rho)$ and corresponding eigenfrequencies ω_n, which can be numbered by integers $n = 1, 2, \ldots$ omitting the azimuthal index $m = 0$ (radial symmetry). We use the index $n = 0$ for the vortex translation mode.[21] This mode has azimuthal indices $m = \pm 1$. We do not assume any boundary conditions for the dynamic magnetization on the dot side boundary due to negligibly small surface anisotropy for soft magnetic materials (FeNi, for instance). The vortex core is a stable formation which is strongly coupled by exchange forces and we assume that the dynamic magnetization has considerable values only outside of the vortex core, in the area where $\Theta_0(\rho) = \pi/2$. Then the dynamic magnetization will have only two components, μ_ρ and μ_z given by Eq. (1), which are perpendicular to the vortex static magnetization $\mathbf{m}_0 = (0, m_0^\phi, 0)$. These components depend on time as $\mu_\rho(t) \sim \sin(\omega t + \phi_0)$, $\mu_z(t) \sim \cos(\omega t + \phi_0)$, where ϕ_0 is an initial phase. This time dependence corresponds to elliptical precession of the dynamic magnetization components in the $\rho - z$ plane around the vortex static equilibrium magnetization $\mathbf{m}_0$. The dynamic μ_ρ component determines the dynamic side surface and volume magnetic charges. The coupled oscillations of μ_ρ and μ_z then lead to a considerable increase of the dynamic magnetostatic energy (mainly due to volume charges, because surface charges described by $\mu_\rho(R)$ magnetization component are small) and to more high eigenfrequencies in comparison with the case of the vortex translation mode (no induced surface charges). Assuming that the dynamic components are concentrated mainly outside of the vortex core, in the area $\Theta_0(\rho) = \pi/2$, for small dot aspect ratio $L/R \ll 1$ (in this case $g_{zz}(\rho, \rho') = -4\pi\delta(\rho - \rho')/\rho$) we get from Eqs. (7) and (8) the simplified integral equation

$$\left(\frac{\omega}{\omega_M}\right)^2 \mu(\rho) = -\frac{1}{4\pi} \int_0^R d\rho' \rho' g_{\rho\rho}(\rho, \rho')\mu(\rho'), \qquad (9)$$

$$g_{\rho\rho}(\rho, \rho') = -4\pi \int_0^\infty dk\, k f(kL) J_1(k\rho) J_1(k\rho'), \qquad (10)$$

$$f(x) = 1 - (1 - e^{-x})/x \quad , \quad \omega_M = \gamma 4\pi M_s.$$

The eigenfrequency ω_n which corresponds to the normalized to unit n-eigenfunction $\mu_n(\rho)$ is

$$\left(\frac{\omega_n}{\omega_M}\right)^2 = -\frac{1}{4\pi}\int_0^R d\rho\rho\int_0^R d\rho'\rho'g_{\rho\rho}(\rho,\rho')\mu_n(\rho)\mu_n(\rho') \tag{11}$$

In this magnetostatic approximation the vortex eigenfrequencies depend only on the dot aspect ratio L/R. More careful analysis shows that the eigenfrequencies are approximately proportional to $\sqrt{L/R}$ if the aspect ratio $\beta = L/R \ll 1$. The solution of the spectral problem Eq. (9) will give us a discrete set of approximate magnetostatic eigenfunctions (radial modes profiles) and eigenfrequencies. The kernel of Eq. (9) is real and can be symmetrized. This means that the Hilbert-Schmidt theory of the integral equations is applicable for our case. The eigenvalues are real and the corresponding eigenfunctions are orthogonal. The approximate numerical solution of the spectral problem (Eq. (9)) for FeNi dot parameters (with $M_s = 800$ G, $\gamma/2\pi = 2.95$ GHz/kOe and $\omega_M/2\pi = 29.7$ GHz) and different L/R gives us the set of eigenfrequencies and eigenfunctions (see Fig. 1, 2, and 3). In the limiting case of a thin dot $\beta \ll 1$ this problem can be solved analytically. We get eigenfrequencies $(\omega_n/\omega_M)^2 = f(\beta\alpha_n)$ and eigenfunctions $\mu_n(\rho) = C_n J_1(\kappa_n\rho)$, where α_n is the nth root of the equation $J_1(x) = 0$, $\kappa_n = \alpha_n/R$, $J_1(x)$ is the first order Bessel function, and C_n is the normalization constant. The set of κ_n can be treated as a set of allowed quantized radial wave numbers, which is consistent with the geometry of a circular dot and its symmetry of the vortex ground state. The equation for κ_n corresponds to the strong pinning on the dot side surface $\rho = R$. In contrast, the numerical solution of Eq. (9) corresponds to some intermediate values of the pinning, although this pinning is strong enough. This pinning is of pure dipolar origin and it was calculated for thin magnetic stripes in Ref. 28. The radial eigenfunctions $J_1(\kappa_n\rho)$ form a complete orthogonal set and can be considered as good trial functions, which are asymptotically exact within the limit $\beta \to 0$. The eigenfrequencies ω_n correspond to dynamic magnetostatic oscillations in the absence of the internal magnetic field.

III. MICROMAGNETIC CALCULATIONS AND DISCUSSION

A. Vortex static configuration

The numerical 3D dynamic micromagnetic simulations are carried out using a hybrid finite element/boundary element method.[29] The nanodots are discretized into tetrahedral finite elements. The magnetic polarization is defined on the nodes of the finite element mesh and linear test functions are used on isoparametric elements. The effective field which is the sum of the exchange, anisotropy, magnetostatic, and external field is calculated directly (for the local contributions from exchange,
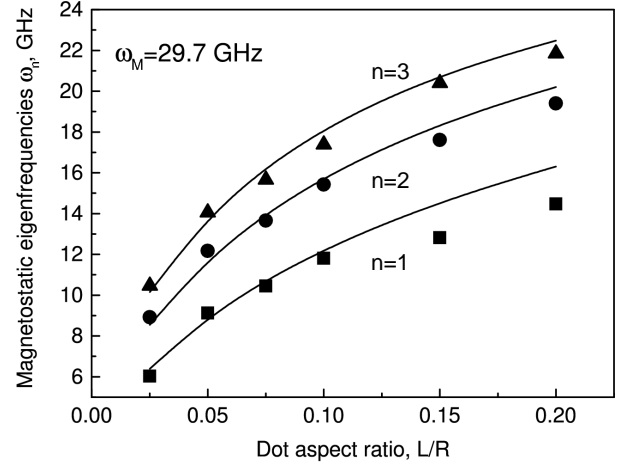

FIG. 1: Dependence of the eigenfrequencies of the vortex radial modes with the indices n=1,2,3 on the dot aspect ratio L/R. The closed symbols correspond to numerical solutions of Eqs. (9) and (10).
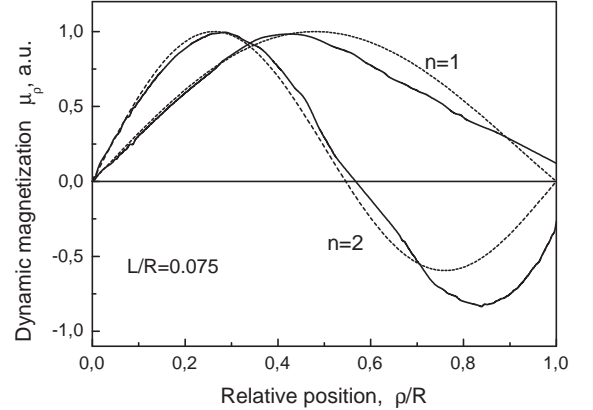

FIG. 2: The vortex radial eigenfunctions $\mu_n(\rho)$ for the dot aspect ratio $\beta = 0.075$ calculated by Eqs. (9) and (10). The solid lines are numerical solutions of Eqs. (9) and (10), the dashed lines are the Bessel functions $J_1(\kappa_n\rho)$.
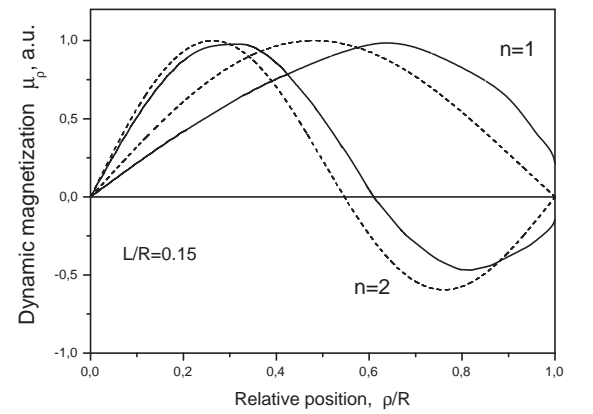

FIG. 3: The vortex radial eigenfunctions $\mu_n(\rho)$ for the dot aspect ratio $\beta = 0.15$. The solid lines are numerical solutions of Eqs. (9) and (10), the dashed lines are the Bessel functions $J_1(\kappa_n\rho)$.
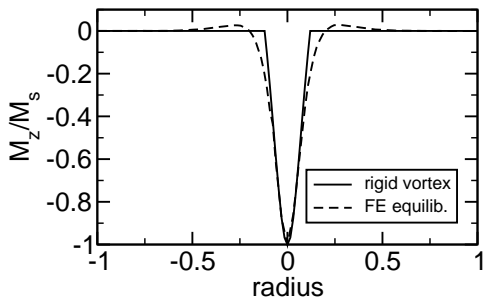
FIG. 4: The calculated profile of the out-of-plane M_z magnetization component in a circular nanodot ($R = 200$ nm, $L = 10$ nm). The solid line is solution of Eq. (1), the dashed line corresponds to finite element micromagnetic simulations.

anisotropy, and external field) as $\mathbf{H}_{\text{eff}} \approx -\partial W/\partial \mathbf{m}$ (W is the energy density in Eq. (3)) and using a boundary element method[30] for the long range magnetostatic field with open boundary conditions. The dynamic Landau-Lifshitz equation of motion for the magnetization is integrated with a preconditioned backward differentiation method.[31,32] For the numerical micromagnetic finite element simulations we have assumed the material parameters of permalloy ($Ni_{80}Fe_{20}$), which is a typical soft magnetic material with negligible magnetocrystalline anisotropy. We set the magnetic saturation polarization to $J_s = \mu_0 M_s \approx 1$ T and the exchange constant to $A = 13 \times 10^{-12}$ J/m, which gives an exchange length $L_{\text{ex}} = \sqrt{2A/M_s^2} = 5.7$ nm.

The finite element simulations have been initialized with the magnetization distribution of the vortex model based on Eq. (1) and an approximate core radius. Then the Landau-Lifshitz equation of motion for the magnetization has been integrated with a damping constant $\alpha = 1$ in zero field, and the magnetization relaxed to its equilibrium distribution, which minimizes the total Gibbs' free energy. The plots of the normal magnetization component M_z in Fig. 4 show a comparison of the analytic vortex model with the equilibrium magnetization distribution of the FE simulation.

We define the vortex core radius by the equation $M_z(\rho) = 0$. The numerical results show, that the vortex core is approximately 50% larger (18.5 nm) than assumed by the vortex model given by Eq. (1) (12 nm). Furthermore the finite element simulation shows that there is a region with $M_z < 0$ outside the core. Thus, we find positive surface charges in the core of the vortex, which are surrounded by negative surface charges. Only outside of approximately half the radius (50 nm) almost all surface charges disappear. It has been verified, that there is very little variation of the magnetization distribution across the thickness of the nanodot. The effect of small oscillations of the static vortex magnetization profile can be neglected for large $R > 200$ nm.

The difference in magnetostatic and exchange energy between the approximate analytical vortex model given by Eq. (1) and the finite element simulation is calculated.
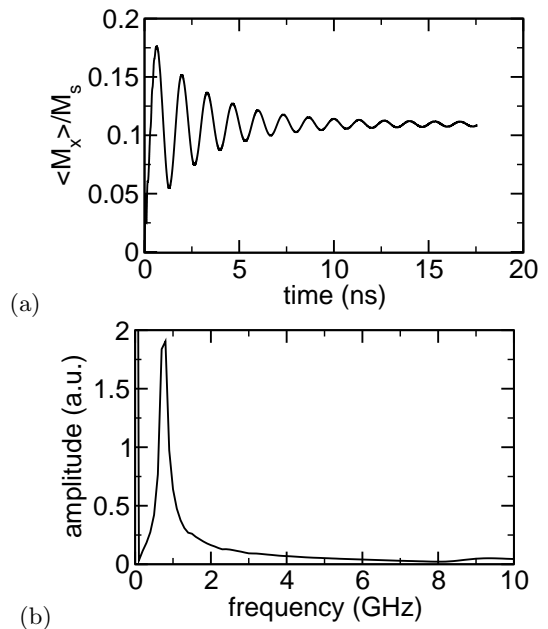

(a)

(b)

FIG. 5: Oscillations of the in-plane averaged vortex magnetization component $\langle M_x \rangle$ as a function of time (a) and its Fourier spectrum (b) for the dot with $L/R = 20$ nm/100 nm $= 0.2$ under applied in-plane field $H_x = 0.01$ T.

The static vortex magnetization distribution within the analytic vortex model has been obtained using the formulas given in Refs. 27 and 33. The equilibrium magnetization distribution after relaxation (dashed line in Fig. 4) as calculated with the finite element model leads to a 4.4% lower total energy. We confirmed numerically that the vortex core has relatively small radius < 20 nm and, therefore, it can be ignored in the description of magnetization dynamics of large dots with $0.2 < R < 2\mu$m.[22,34]

B. Vortex translation mode

To study the vortex lowest frequency mode (translation mode) numerically an external field of 10 mT has been applied in the plane of the dot to the remanent state and a damping constant of $\alpha = 0.05$ has been assumed. The time evolution of $\langle M_x \rangle$ (the average of M_x over the whole nanodot) for a dot with an aspect ratio of $L/R = 10$ nm/100 nm $= 0.1$ is given in Fig. 5(a). Then the damped oscillation, which is caused by the spiral motion of the vortex core towards its equilibrium position, is observed. The corresponding Fourier spectrum is given in Fig. 5(b) and shows a sharp peak at a frequency of 0.7 GHz.

Fig. 6 shows the results of calculations of the translation mode eigenfrequencies of various nanodots with a radius $R = 100$ nm and a thickness between 10 and 40 nm. The translation eigenfrequency is approximately linearly proportional to the dot aspect ratio L/R. The results are in good agreement with the results of a finite
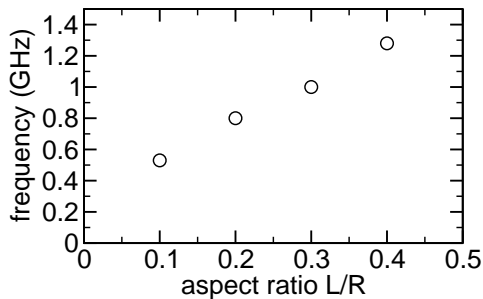
FIG. 6: Translation mode eigenfrequency versus the dot aspect ratio L/R for cylindrical nanodots with $R = 100$ nm.
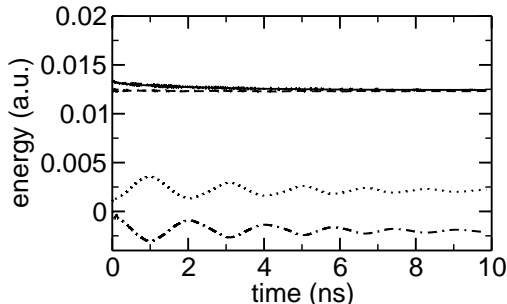

FIG. 7: The contributions to magnetic energy vs. time for a cylindrical dot with $L/R = 0.1$ and $H_x = 0.01$ T. Solid line: the total magnetic energy, dashed line: exchange energy, dotted line: magnetostatic energy, dot-dashed line: Zeeman energy.

difference model and the analytical "two-vortices" model presented in Ref. 21.

The decreasing total energy (dissipation due to damping with $\alpha = 0.05$ in the Landau-Lifshitz equation of motion) and the swapping between magnetostatic and Zeeman energy are shown in Fig. 7. The exchange energy remains constant, because the vortex core, which accounts for most of the exchange energy, moves without changing its shape. This supports the analytical description of the translational mode suggested in Ref. 21, where circular motion of the vortex core as whole was calculated. Note that recently existence of this low-frequency vortex translation mode was confirmed experimentally by direct Kerr microscopy measurements in Ref. 35. The eigenfrequency measured by Park et al. agrees with our calculations with an error of less than 20%.

C. Vortex radial modes

The vortex radial modes were excited by applying an external field of 5 mT in z-direction and relaxing the magnetization with large damping ($\alpha = 1$). When equilibrium was reached, the external field was instantaneously switched off and the free oscillation in zero field with very low damping was studied. With $\alpha = 0.05$ the oscillations are damped out within a few oscillations. As
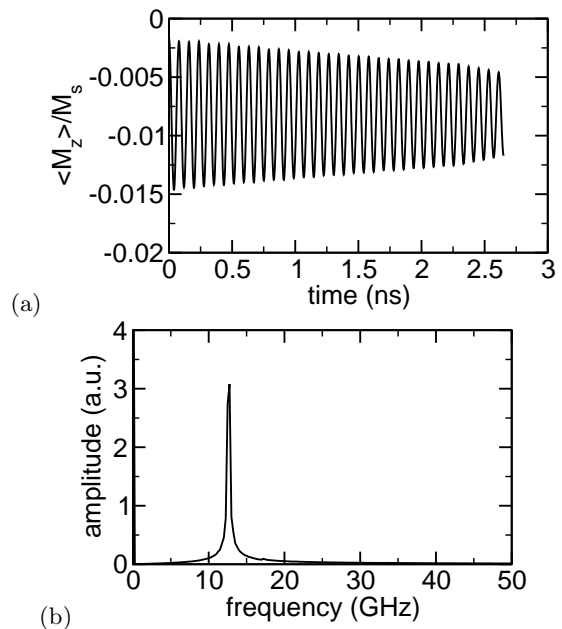

FIG. 8: Oscillations of the averaged out-of-plane magnetization component $\langle M_z \rangle$ as a function of time (a) and its Fourier spectrum (b) for the cylindrical dot with $L/R = 0.2$ under applied out-of-plane field $H_z = 0.005$ T.

a result the Fourier spectra are very poor because the resolution of the Fourier spectra increases with measurement time. Therefore $\alpha = 0.001$ has been used to observe many oscillations and obtain a high resolution Fourier spectrum.

The time dependence of the average magnetization $\langle M_z \rangle$ and the Fourier spectra for nanodots with an aspect ratio of $L/R = 20$ nm/100 nm $= 0.2$ and $L/R = 40$ nm/200 nm $= 0.2$ are given in Figs. 8(a) and (b) and 9(a) and (b), respectively. Note that the azimuthal modes (with the index $m \neq 0$) do not contribute to oscillations of $\langle M_z \rangle$. We checked numerically that the calculated modes have radial symmetry and correspond to the rotation of the dynamical magnetization $\mu = (\mu_\rho, 0, \mu_z)$ around the vortex static magnetization $\mathbf{m}_0 = (0, m_0^\phi, 0)$ (cf. Fig. 10).

For the constant aspect ratio $L/R = 0.2$ we find an eigenfrequency of approximately 12.6 GHz. However, for a nanodot with $L/R = 40$ nm/200 nm $= 0.2$ a very pronounced beating is observed (Fig. 9). This is due to the fact, that there is another eigenfrequency of 11.6 GHz very close to the 12.6 GHz oscillation. However, the main peak position depends only on the combination ratio L/R. This confirms the magnetostatic origin of the mode. But the physical picture is more complicated for large L, when the magnetization dependence on z may be essential.

We concentrated on numerical simulations of the dependence of the first magnetostatic radial eigenfrequency on the dot aspect ratio L/R. The calculated evolution of the first radial mode with increasing dot thickness L
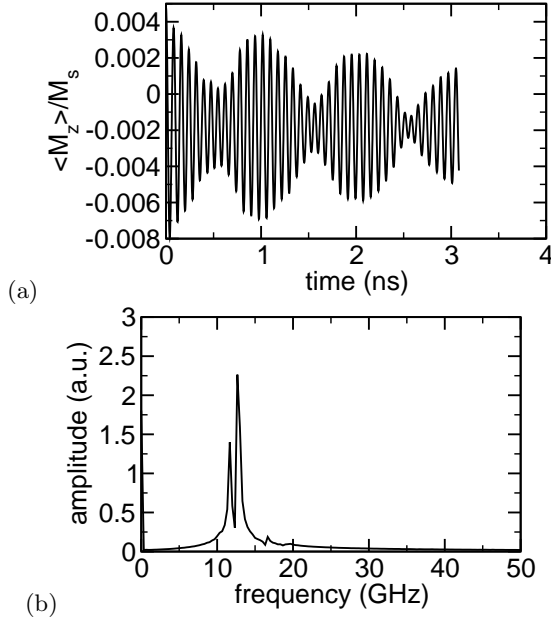
FIG. 9: Oscillations of the averaged out-of-plane magnetization component $\langle M_z \rangle$ as a function of time (a) and its Fourier spectrum (b) for the cylindrical dot with $L/R = 40$ nm/200 nm = 0.2.
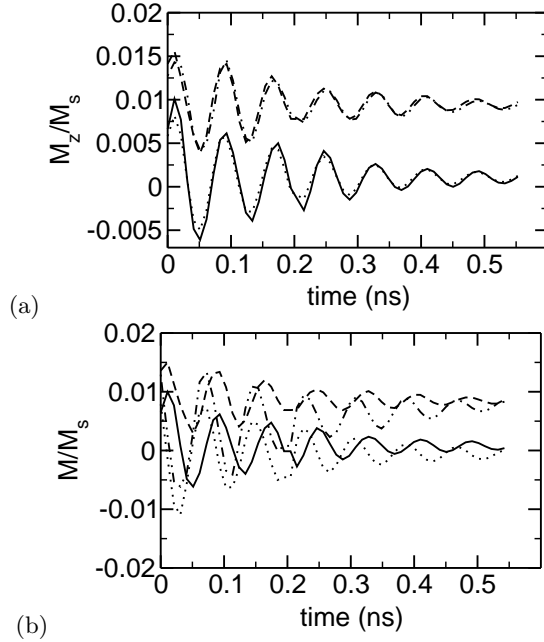

FIG. 10: Oscillations of the vortex magnetization components. (a) M_z (measured at different positions $\xi = x/R$, solid line: $\xi = -1$, dotted line: $\xi = -0.8$, dashed line: $\xi = -0.5$, dot-dashed line: $\xi = +0.5$) oscillates in phase across the whole nanodot. The oscillation amplitude slightly decreases towards the center. (b) M_ρ and M_z as a function of time at different radii $r = \rho/R$. Solid line: M_z at $r = 1.0$, dotted line: M_ρ at $r = 1.0$, dashed line: M_z at $r = 0.5$, dot-dashed line: M_ρ at $r = 0.5$). The phase shift between the M_ρ and M_z components is equal to 90 deg (magnetization rotation in the z-ρ plane).
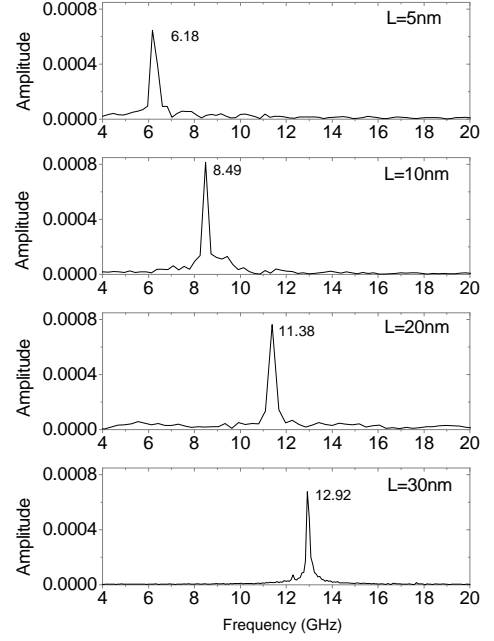

FIG. 11: Evolution of the Fourier spectrum of the component $\langle m_z \rangle$ for the first ($n = 1$) radial vortex excitation mode with varying the dot thickness L from 5 nm to 30 nm. $R = 200$ nm.
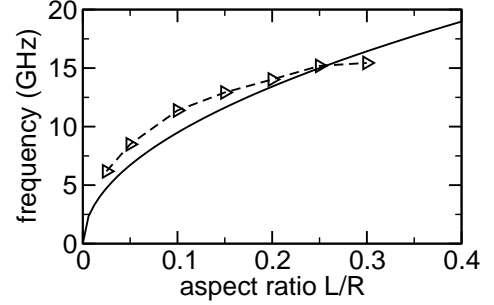

FIG. 12: The radial vortex mode eigenfrequencies versus aspect ratio L/R for nanodots with different thickness L. The open triangles are points simulated numerically, the solid line corresponds to fitting using the equation $\omega_n \sim \sqrt{L/R}$.

(5-30 nm) is shown in Fig. 11. The eigenfrequency of this mode increases with L in agreement with analytical calculations of the vortex magnetostatic modes in Sec. II. We plotted the micromagnetically simulated eigenfrequency as a function of the dot aspect ratio L/R in Fig.12 together with the analytic dependence $\omega_n \sim \sqrt{L/R}$ and got a good agreement of the eigenfrequencies calculated by these different methods. Thus, our numerical calculations confirmed that the radial eigenfunctions and eigenfrequencies which correspond to low-lying part of the vortex dot excitation spectrum have magnetostatic origin.

The calculated radial eigenmodes are magnetostatic (wave length is of the order of the dot radius) and concentrated in the area outside of the vortex core (see Figs. 2, 3

for the calculated eigenfunctions). The eigenfrequencies of these modes ω_n are determined by the dynamic demagnetizing fields. The static dipolar field for the vortex structure has two components H_z and H_ρ, which depend on ρ only due to circular symmetry of the vortex. Both components are negligibly small in the area of our interest, i.e. outside the vortex core. In this sense the problem of non-uniform magnetostatic spin-excitations is similar to the problem of magnetostatic waves in thin magnetic stripes magnetized along their long side considered by Guslienko et al. in Ref. 28. Effective boundary conditions for dynamic magnetization on the dot surface side can be also formulated similarly to Ref. 28. The condition $\mu_n(\rho = 0) = 0$ is satisfied near the dot center. This is consistent with our assumption about concentration of the dynamic magnetization of the radial modes outside the vortex core. These radially symmetric magnetic dynamic excitations can be detected by modern experimental techniques such as BLS, FMR, and time-resolved Kerr- and magnetic circular dichroism measurements.

Very recently, when this manuscript was ready for submission, we became aware of experimental data by Buess et al.[36] They measured the eigenfrequencies of the vortex radial modes by time-resolved Kerr microscopy and obtained frequencies of 2.8, 3.9 and 4.5 GHz. The dot aspect ratio $\beta = L/R = 15$ nm/3000 nm $= 0.005$ is very small and we can apply the approximate equation $(\omega_n/\omega_M)^2 = f(\beta\alpha_n)$ derived from Eq. (11). The calculated eigenfrequencies 2.91, 3.93 and 4.73 GHz are very close to the experimental data.

IV. CONCLUSIONS

The vortex eigenfrequencies and magnetization profiles were calculated on the basis of analytical and numerical approaches. The low-lying part of the spectrum of spin excitation over the vortex ground state consists of discrete eigenfrequencies of magnetostatic origin. The corresponding dynamic eigenmodes are localized near the dot center (the lowest translation mode) or are excited mainly outside the vortex core (radially symmetric magnetostatic modes). The model of the shifted vortex with no side surface charges[21] well explains the results of our micromagnetic numerical calculations of the translation mode eigenfrequency. The set of magnetostatic eigenfunctions $\mu_n(\rho)$ and eigenfrequencies ω_n was calculated as a function of the dot aspect ratio L/R. The first magnetostatic eigenfunction can be approximately described as a uniform mode (no nodes). Whereas the high frequency eigenfunctions have a number of the nodes proportional to their number. The frequencies of the radial eigenmodes are proportional to $\sqrt{L/R}$ for thin magnetic dots with dot thickness $L \approx L_{\mathrm{ex}}$ and dot radii of about $1~\mu$m.

* Electronic address: gusliyenko@anl.gov

1 A. Lyberatos, G. Ju, R. J. M. van de Veerdonk, and D. Weller, J. Appl. Phys. **91**, 2236 (2002).

2 O. Chubykalo, J. D. Hannay, M. Wongsam, R. W. Chantrell, and J. M. Gonzalez, Phys. Rev. B **65**, 184428 (2002).

3 C. A. Ross, Annu. Rev. Mater. Res. **31**, 203 (2000).

4 C. A. Ross, M. Hwang, M. Shima, J. Y. Cheng, M. Farhoud, T. A. Savas, H. I. Smith, W. Schwarzacher, F. M. Ross, M. Redjdal, et al., Phys. Rev. B **65**, 144417 (2002).

5 T. Shinjo, T. Okuno, R. Hassdorf, K. Shigeto, and T. Ono, Science **289**, 930 (2000).

6 J. Raabe, R. Pulwey, R. Sattler, T. Schweinböck, J. Zweck, and D. Weiss, J. Appl. Phys. **88**, 4437 (2000).

7 M. Schneider, H. Hoffmann, and J. Zweck, Appl. Phys. Lett. **77**, 2909 (2000).

8 R. P. Cowburn, D. K. Koltsov, A. O. Adeyeye, M. E. Welland, and D. M. Tricker, Phys. Rev. Lett. **83**, 1042 (1999).

9 V. Novosad, K. Guslienko, H. Shima, Y. Otani, K. Fukamichi, N. Kikuchi, O. Kitakami, and Y. Shimada, IEEE Trans. Magn. **37**, 2088 (2001).

10 V. Novosad, M. Grimsditch, K. Y. Guslienko, P. Vavassori, Y. Otani, and S. D. Bader, Phys. Rev. B **66**, 052407 (2002).

11 K. Y. Guslienko, V. Novosad, Y. Otani, H. Shima, and K. Fukamichi, Phys. Rev. B **65**, 024414 (2002).

12 A. M. Kosevich, B. A. Ivanov, and A. S. Kovalev, Phys. Reports **194**, 117 (1990).

13 K. Y. Guslienko, V. Novosad, Y. Otani, H. Shima, and K. Fukamichi, Appl. Phys. Lett. **78**, 3848 (2001).

14 K. Y. Guslienko and K. L. Metlov, Phys. Rev. B **63**, 100403(R) (2001).

15 R. P. Cowburn, J. Phys. D: Appl. Phys. **33**, R1 (2000).

16 A. Fernandez and C. J. Cerjan, J. Appl. Phys. **87**, 1395 (2000).

17 M. Grimsditch, Y. Jaccard, and I. K. Schuller, Phys. Rev. B **58**, 11539 (1998).

18 D. K. Koltsov, R. Cowburn, and M. E. Welland, J. Appl. Phys. **88**, 5315 (2000).

19 W. K. Hiebert, A. Stankiewicz, and M. R. Freeman, Phys. Rev. Lett. **79**, 1134 (1997).

20 Y. Acremann, C. H. Back, M. Buess, O. Portmann, A. Vaterlaus, D. Pescia, and H. Melchior, Science **290**, 492 (2000).

21 K. Y. Guslienko, B. A. Ivanov, V. Novosad, Y. Otani, H. Shima, and K. Fukamichi, J. Appl. Phys. **91**, 8037 (2002).

22 B. A. Ivanov and C. Zaspel, J. Appl. Phys. **95**, 7444 (2004).

23 B. E. Argyle, E. Terrenzio, and J. C. Slonczewski, Phys. Rev. Lett. **53**, 190 (1984).

24 K. Y. Guslienko and A. N. Slavin, J. Appl. Phys. **87**, 6337 (2000).

25 J. Jorzick, C. Krämer, S. O. Demokritov, B. Hillebrands,

B. Bartenlian, C. Chappert, D. Decanini, F. Rousseaux, E. Cambril, E. Søndergard, et al., J. Appl. Phys. **89**, 7091 (2001).

[26] B. A. Ivanov, H. J. Schnitzer, F. G. Mertens, and G. M. Wysin, Phys. Rev. B **58**, 8464 (1998).

[27] N. A. Usov and S. E. Peschany, J. Magn. Magn. Mater. **118**, L290 (1993).

[28] K. Y. Guslienko, S. O. Demokritov, B. Hillebrands, and A. N. Slavin, Phys. Rev. B **66**, 132402 (2002).

[29] J. Fidler and T. Schrefl, J. Phys. D: Appl. Phys. **33**, R135 (2000).

[30] D. R. Fredkin and T. R. Koehler, IEEE Trans. Magn. **26**, 415 (1990).

[31] S. D. Cohen and A. C. Hindmarsh, Computers in Physics **10**, 138 (1996).

[32] D. Suess, V. Tsiantos, T. Schrefl, J. Fidler, W. Scholz, H. Forster, R. Dittrich, and J. J. Miles, J. Magn. Magn. Mater. **248**, 298 (2002).

[33] N. A. Usov and S. E. Peschany, Fiz. Met. Metalloved (transl.: The Physics of Metals and Metallography) **12**, 13 (1994).

[34] W. Scholz, K. Y. Guslienko, V. Novosad, D. Suess, T. Schrefl, R. W. Chantrell, and J. Fidler, J. Magn. Magn. Mater. **266**, 155 (2003).

[35] J. P. Park, P. Eames, D. M. Engebretson, J. Berezovsky, and P. A. Crowell, Phys. Rev. B **67**, 020403(R) (2003).

[36] M. Buess, R. Höllinger, T. Haug, K. Perzlmaier, U. Krey, D. Pescia, M. R. Scheinfein, D. Weiss, and C. H. Back, Phys. Rev. Lett. **93**, 077207 (2004).